Journal of Biomedical Optics

SPIEDigitalLibrary.org/jbo

Mosaic acquisition and processing for optical-resolution photoacoustic microscopy

Peng Shao
Wei Shi
Ryan K. W. Chee
Roger J. Zemp

SPIE

Mosaic acquisition and processing for optical-resolution photoacoustic microscopy

Peng Shao, Wei Shi, Ryan K. W. Chee, and Roger J. Zemp
University of Alberta, Department of Electrical & Computer Engineering, Edmonton T6G2V4, Canada

Abstract. In optical-resolution photo-acoustic microscopy (OR-PAM), data acquisition time is limited by both laser pulse repetition rate (PRR) and scanning speed. Optical-scanning offers high speed, but limited, field of view determined by ultrasound transducer sensitivity. In this paper, we propose a hybrid optical and mechanical-scanning OR-PAM system with mosaic data acquisition and processing. The system employs fast-scanning mirrors and a diode-pumped, nanosecond-pulsed, Ytterbium-doped, 532-nm fiber laser with PRR up to 600 kHz. Data from a sequence of image mosaic patches is acquired systematically, at predetermined mechanical scanning locations, with optical scanning. After all imaging locations are covered, a large panoramic scene is generated by stitching the mosaic patches together. Our proposed system is proven to be at least 20 times faster than previous reported OR-PAM systems.
[DOI: 10.1117/1.JBO.17.8.080503]

Keywords: microscopy; photo-acoustic imaging; mosaicing.

Paper 12290L received May 9, 2012; revised manuscript received Jun. 16, 2012; accepted for publication Jun. 29, 2012; published online Jul. 19, 2012.

Optical-resolution photo-acoustic microscopy (OR-PAM) is a novel imaging modality for visualizing optically absorbing structures with high lateral resolution provided by fine optical focusing. Since proposed by Maslov et al.,[1] it has been applied to both morphological and functional imaging in biological subjects. The technique was used to image microcirculation at the capillary level,[2] brain micro-vascular morphology and oxygenation,[3] amyloid plaques in Alzheimer's disease mouse models,[4] ocular micro-vasculature,[5] and healing processes of laser-induced lesions in small animal models.[6] Recently, Tsytsarev et al.[7] used OR-PAM to monitor micro-vascular response to electrical stimulations of living mouse somatosensory cortex with exposed cranium.

Data acquisition time is limited by scanning speed, laser pulse repetition rate (PRR), and data transfer. Different raster scanning schemes were introduced, among which, the most commonly used is to mechanically translate the bulky imaging head within the horizontal x-y plane[1–7] while firing laser pulses and periodically receiving photo-acoustic signals. Considerable data acquisition time is unavoidable in this case. Hu et al.[8] reported that with their recently developed, second generation (G2) OR-PAM system, 70 min is needed to scan a mouse ear with an area of 7.8×10 mm. While stunning image quality was demonstrated, acceptance of the imaging modality, in practical applications, is hampered by the long data acquisition time.

Optical scanning was introduced, by Xie et al.,[9] to prevent mechanical scanning and to speed up the imaging process. While the laser beam raster scan was achieved by an x-y galvanometer scanner, an unfocused transducer was used to sense the generated photo-acoustic signals. Utilizing a laser system with PRR of 1024 Hz, data acquisition time for a 256×256-pixels image was reported as less than 2 min. Although a large circular field of view (FOV) of 6-mm diameter was demonstrated, a trade-off between signal to noise ratio (SNR) and FOV always exists. A hybrid-scanning OR-PAM (HSOR-PAM) scheme was used by Rao et al.[10] With this setup, fast scanning was achieved with a galvanometer mirror along one axis and mechanical scanning was accomplished using a 1D mechanical translation stage along the other axis. A cylindrically-focused transducer was used to receive ultrasonic signals. Using a laser system with a PRR of 5 kHz, the system required 256 s to obtain an $800 \times 1600 \times 200$ volumetric data set of live mouse ear vasculature. SNR of the imaging system was somewhat compromising middle ground between the optical scanning scheme of Xie[9] and mechanical scanning methods.[1,8] Scanning range along the fast scan direction is limited. Furthermore, motion artifacts might be a potential problem when imaging a large area with this setup. Wang et al.[11] developed a voice-coil scanning system that is able to accomplish B-scan in a range of 1 mm at 40 and 20 Hz at a range of 9 mm. Scanning in the other axis is achieved with a mechanical motor stage. Some of these system architectures could perform faster with a higher repetition rate laser. However, for the hybrid and optical scanning systems, the FOV will be limited in at least one direction. Mechanical scanning will limit the image speed of G1 and G2 OR-PAM systems.

In this letter, we describe a fast OR-PAM system engineered for providing large FOV using mosaic acquisition and data processing. In this system, a three-axis stepper-motor subsystem is used to mechanically move the target to be imaged from patch-to-patch in less than 0.5 s. Patch images are aligned and stitched to generate a large scene composite. Our proposed system, which is a hybrid approach between laser-scanning and mechanical scanning, retains the SNR-advantages of focused-transducer OR-PAM systems we recently introduced.[12]

Configuration of our system is illustrated in Fig. 1. We use a diode-pumped, pulsed, Ytterbium-doped, fiber laser system as the optical source (GLP-10, IPG Photonics Corporation), which generates 532-nm output pulses with durations of ~1 ns, and the pulse energy can reach as high as 20 μJ. The PRR of the laser pulses is tunable within the range of 20 to 600 kHz. A glass slide is used to reflect a small amount of light to a photodiode and to be used as a trigger for data acquisition. Optical scanning is achieved by a pair of galvanometer mirrors (6230H, Cambridge Technology Inc.) driven by two sinusoidal waves (x-y) from a function generator (Tektronix ATG 3022B). Scanning range, or FOV, of one individual image is determined by the amplitude of the sinusoidal signals. The scanned beam is focused by an objective lens (NA = 0.15, Thorlabs Inc.) with a focal length of 18 mm and then travels through our custom designed,

Address all correspondence to: Roger J. Zemp, University of Alberta, Department of Electrical & Computer Engineering, Edmonton T6G2V4, Canada. Tel: 1-(780) 492-1825; Fax: 1-(780)492-1811; E-mail: rzemp@ualberta.ca

0091-3286/2012/$25.00 © 2012 SPIE

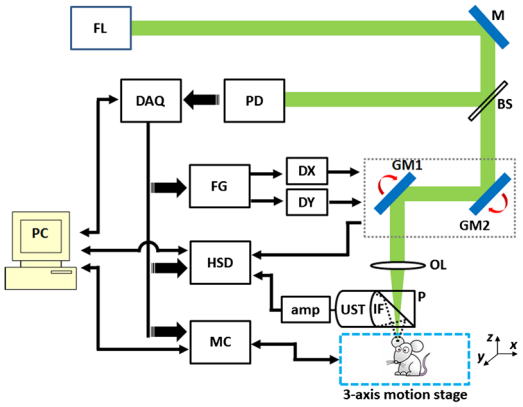

Fig. 1 System configuration. FL: fiber laser; M: mirror; BS: beam-splitter; GM1, GM2: Galvanometer mirrors; PD: photo-diode; DAQ: data acquisition card; FG: function generator; DX/DY: mirror drivers; HSD: high-speed digitizer; MC: motion card; amp: amplifier; UST: ultrasound transducer; IF: index-matching fluid; P: prism;

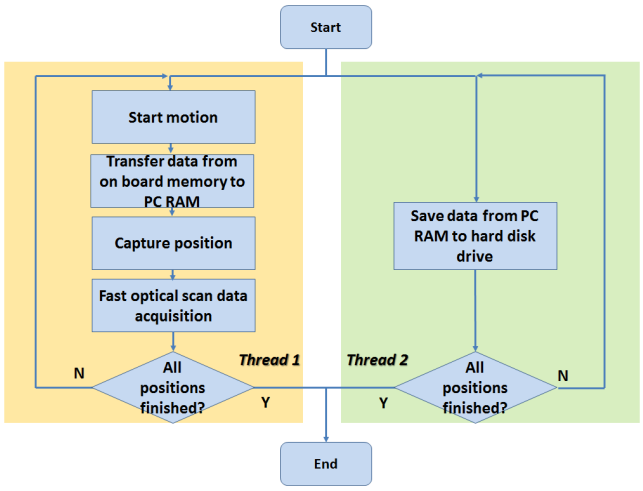

Fig. 2 Flow chart of the control software. One thread is used to coordinate photoacoustic data acquisition, while the other thread is generated to save data into the PC hard-drive.

low-loss, light-delivery probe[12] before reaching the imaging object. A 3.5 MHz ultrasound transducer (SLIG 3-02, CD International Technology, Inc.), with a 19-mm focal length and 6-mm active element, is employed to sense photo-acoustic signals.

An 8-channel, 12-bit, PCI high speed digitizer (CS8289, Gage Applied Technologies Inc.) is used for data collection. Two channels of the HSD card are used to digitize and store photo-acoustic signals and the scanning sinusoidal feedback signal with the higher frequency (x-axis). A pulser-receiver (5900 PR, Olympus NDT Inc.) is used for photo-acoustic signal amplification and prefiltering.

The object to be imaged is mounted on a motorized, high precision, three-axis, motion stage to realize mosaic movement. A PCI motion card (NI 7350) is utilized to communicate with the motion system that consists of three integrated high torque stepper motors (23Y002D-LW8, Anaheim Automation).

Mosaic acquisition is accomplished by acquiring small FOV, fast-optical scans, successively, in a sequence of mosaic patches at mechanically-scanned 2D grid locations. The object is moved to each mosaic location until the entire region is covered. At each imaging spot, the location of the stage is sensed by encoders and recorded for patch alignment. Stage movement, data collection, and optical scanning are coordinated with a square wave generated by a DAQ card (NI PCI 6221, National Instruments) which shares the same frequency as the slow-axis (y-axis) scanning signal. Photo-acoustic data acquisition is active only for the backward portion of the y-axis signal. During data acquisition, the low-phase of the coordinating square wave is used to inhibit the motors to avoid electronic noise from the motion subsystem. After each mosaic data acquisition is complete and during stepper motor activation for subsequent patch positioning, data from the previous patch is transferred from the HSD-card, on-board memory to a number of preallocated data buffers in the random-access memory (RAM) of the PC. The buffers are created when commencing the imaging task and utilized in a circular pattern to minimize system resource requirements. A separate thread manages to save data from PC RAM to the hard drive when buffers are not empty. Software for realizing data collection and motion control is written in C/C++. A flowchart of the control software is illustrated in Fig. 2. Multiple threading is used to coordinate tasks such as data acquisition, stage movement and data saving.

Scanning areas, for each subimage, is intentionally kept larger than desired mosaic patch sizes. Image redundancy permits position shifts for image alignments to account for motion artifacts and also helps improve SNR in the marginal area of each small FOV scene. In data processing, mosaic patches are first positioned at corresponding locations on the 2D grid system then shifted according to the position feedback information obtained during the imaging process to compensate mechanical movement errors. Raster scanning directions are aligned to be parallel with the movement directions, therefore, no complex image registration methods are required by this system. Image blending is essential for generating the large composite. We use the feathering[13] method to merge adjacent image mosaic patches. The pixel value at location (x, y) in the new image composite in the overlapping area is determined with the contribution of the two adjacent mosaic patches:

$$N(x, y) = \alpha I_A(x, y) + (1 - \alpha) I_B(x, y).$$

In which $N(x, y)$ is the pixel value in the new image composite at (x, y), $I_A(x, y)$ and $I_B(x, y)$ are the pixel values of adjacent image A and B, respectively. α, the weighting function, h is simply calculated as the distance from image y. This helps eliminate the edge artifacts in the composite image.

Figure 3 shows results of our phantom study. Thirty six images, with a small FOV of $\sim 930 \times 930\ \mu m^2$, were generated in total, as is shown in Fig. 3(a). The mosaic patches were then shifted according to the position feedback information and then stitched to generate the panoramic scene, as shown in Fig. 3(b).

We imaged the blood vessel structures of a 7-week old SCID Hairless Outbred (SHO™, Charles River, MA) mouse ear for

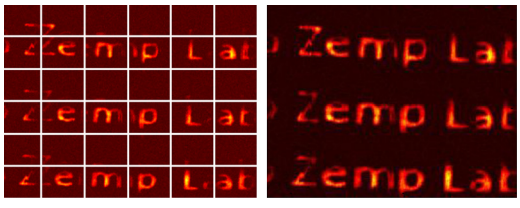

Fig. 3 Phantom studies. (a) 36 Sub-images acquired at a 2D grid locations; (b) image composite generated with the mosaic images with image alignment and stitching.

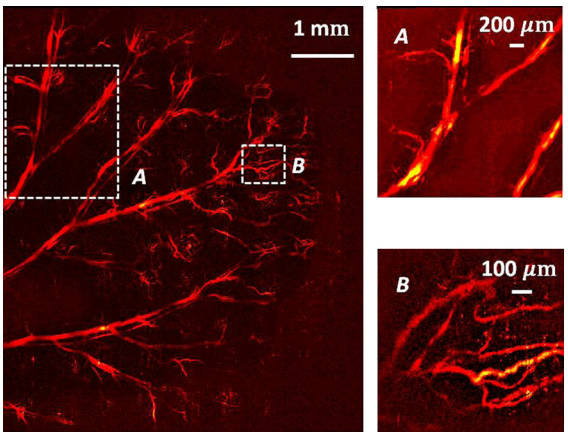

Fig. 4 Micro-vasculature of a living mouse ear. Left: large image composite of the living mouse ear with FOV of 6.45×5.81 mm^2; Upper right: a separate image of the same area framed with dashed box A in the image composite; Bottom right: a magnified individual patch taken from the image composite enclosed by the dash box B.

in vivo studies. All experimental procedures are in conformity with the laboratory animal protocol approved by the Animal Use and Care Committee of the University of Alberta. The mouse was under anesthesia during the imaging process.

The panoramic scene, with an overall area of 6.45×5.8 mm^2, is shown in Fig. 4(a). Ninety (9×10) image mosaics were generated to composite the large FOV image. Distance between imaging spots is 645 μm and the original dimension of image mosaic is around 930×930 μm^2. Figure 4(b) is an image composite with 4×4 image blocks, which is an image of the framed area ***A*** in Fig. 4(a), but acquired separately after the animal was repositioned. The vascular structures in Fig. 4(b) are consistent with those in the region ***A*** shown in Fig. 4(a). To examine the image capability of our system, we take an individual image patch, which is shown in Fig. 4(c) from the large scene. With a fine resolution of around 6 μm of the system,[12] detailed capillary structures can be resolved.

PRR of the laser system is 320 kHz for the imaging experiment. The measured pulse energy after the scanning mirror is ~0.15 μJ. No damage was observed on the animal skin surface after imaging. Assuming that the laser focal spot is around 120 μm beneath the skin surface, the calculated laser fluence on the skin is 18 mJ/cm^2. This is less than the 20 mJ/cm^2 standard by American National Standards Institute (ANSI).We used 400 Hz (x-axis) and 1 Hz (y-axis) sinusoidal waves to drive the scanning mirrors, respectively. Therefore, the B-scan frame rate across 930 μm is 400 Hz. Only 0.5 s is needed to collect data for one mosaic patch with 160,000 pixels (400×400). In total, only 1 s is required for one image mosaic including data acquisition, transfer and the stage movement.

Several advantages of our mosaicing scheme should be noted. First, as a hybrid scanning approach between optical scanning and mechanical scanning, moscaicing significantly speeds up the data acquisition time of the imaging modality. With 320 kHz fiber laser, our system outperforms the G2 OR-PAM, which is introduced by Hu et al.,[8] in terms of data acquisition speed. To scan a region of 7.8×10 mm^2, 70 min is required for G2 OR-PAM, whereas, with the proposed system, only 90 s is needed for a region of 6.45×5.8 mm^2. Our system is at least 20 times faster than G2 in terms of data acquisition time per unit area. Since our system has similar pixel size with G2 OR-PAM, it still surpasses G2 OR-PAM by the same factor if compared with size of dataset per unit time range. Our system is also faster than existing systems with different scanning schemes in terms of dataset size, as discussed above. This speed advantage will prove important for ease of use for end-users. Second, the mosaicing scheme significantly enlarged the FOV possible with optical-scanning OR-PAM, which is limited by the transducer focal waist. Third, since each mosaic patch is acquired in less than 0.5 s, motion artifacts per patch should be minimal and motion artifacts between different mosaic patches can be compensated for by simple image processing. This scheme may be less prone to motion artifacts over large FOVs compared to other mechanical or hybrid-scanning methods.[10] Future work should validate robustness to motion in clinical scenarios. Finally, the mosaicing scheme enables multi-scale imaging with OR-PAM. As shown in Fig. 4(a) and 4(b), one can conduct a rough scan in a larger area for preliminary study and then direct the imaging system to a specific region of interest for further studies after re-adjusting the system in terms of focusing, etc. We believe the aforementioned merits will accelerate the acceptance of the imaging technique among biologists and clinicians.

Acknowledgments

We gratefully acknowledge funding from the Canadian Cancer Society (CCS 2011-700718), NSERC (355544-2008, 375340-2009, STPGP 396444), the Canada Foundation for Innovation Leaders Opportunity Fund (18472), and Alberta Advanced Education & Technology Small Equipment Grants Program (URSI09007SEG). We also acknowledge student scholarship support from Alberta Innovates, NSERC, the Marlene and George Squires Cancer Research Summer Studentship, and the China Scholarship Council.

References

1. K. Maslov et al., "Optical-resolution photoacoustic microscopy for in vivo imaging of single capillaries," *Opt. Lett.* **33**(9), 929–931 (2008).
2. S. Hu, K. Maslov, and L. V. Wang, "Noninvasive label-free imaging of microhemodynamics by optical-resolution photoacoustic microscopy," *Opt. Express* **17**(9), 7688–7963 (2009).
3. S. Hu et al., "Functional transcranial brain imaging by optical-resolution photoacoustic microscopy," *J. Biomed. Opt.* **14**(4), 040503 (2009).
4. S. Hu et al., "Intravital imaging of amyloid plaques in a transgenic mouse model using optical-resolution photoacoustic microscopy," *Opt. Lett.* **34**(24), 3899–3901 (2009).
5. S. Hu et al., "Label-free photoacoustic ophthalmic angiography," *Opt. Lett.* **35**(1), 1–3 (2010).
6. S. Hu, K. Maslov, and L. V. Wang, "*In vivo* functional chronic imaging of a small animal model using optical-resolution photoacoustic microscopy," *Med. Phys.* **36**(6), 2320–2323 (2009).
7. V. Tsytsarev et al., "Photoacoustic microscopy of microvascular responses to cortical electrical stimulation," *J. Biomed. Opt.* **16**(7), 076002 (2011).
8. S. Hu et al., "Second-generation optical-resolution photoacoustic microscopy," *Opt. Lett.* **36**(7), 1134–1136 (2011).
9. Z. X. Xie et al., "Laser-scanning optical-resolution photoacoustic microscopy," *Opt. Lett.* **34**(12), 1771–1773 (2009).
10. B. Rao et al., "Hybrid-scanning optical-resolution photoacoustic microscopy system for in vivo vasculature imaging," *Opt. Lett.* **35**(10), 1521–1523 (2010).
11. L. Wang et al., "Fast voice-coil scanning optical-resolution photoacoustic microscopy," *Opt. Lett.* **36**(2), 139–141 (2011).
12. W. Shi et al., "In vivo near-realtime volumetric optical resolution photoacoustic microscopy using a high-repetition-rate nanosecond fiber-laser," *Opt. Express* **19**(18), 17143–17150 (2011).
13. R. Szeliski, "Video mosaics for virtual environments," *IEEE Compt. Graph. & App.* **16**(2), 22–30 (1996).